Electronic Supplementary Material (ESI) for Physical Chemistry Chemical Physics.

Supporting Information for "Size-dependent formation of membrane nanotubes: Continuum modeling and molecular dynamics simulations"

Falin Tian, Tongtao Yue, Wei Dong, Xin Yi,* and Xianren Zhang*

E-mail: xyi@pku.edu.cn; zhangxr@mail.buct.edu.cn

The parameters a_{ij} chosen for the DPD simulations are in the unit of ε/r_c, where ε is the energy unit and r_c is the cutoff radius for the interaction. Values of a_{ij} can be found in Table S1.

Table S1: Values of interaction parameter a_{ij} between two beads in DPD simulations.

	lipid head	lipid tail	lower surface of nanoplate	upper surface of nanoplate	water
lipid head	25	200	10	30	25
lipid tail	200	25	200	200	200
low surface of nanoplate	10	200	25	25	30
upper surface of nanoplate	30	200	25	25	25
water	25	200	30	25	25

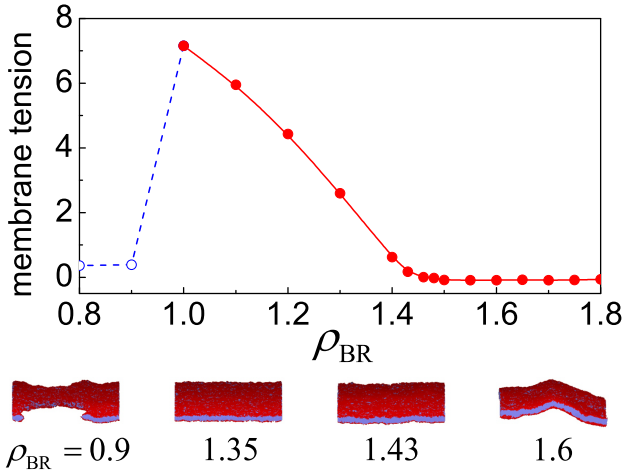

Figure S1: The membrane tension as a function of the lipid number density ρ_{BR}, and selected membrane morphologies at different $\rho_{BR} = 0.9$, 1.35, 1.43, and 1.6. The lipid membrane would rapture at ρ_{BR} ranging from 0.8 to 1.0.

To investigate the relationship between the membrane tension and the lipid number density, we perform N-varied DPD simulations and calculate the membrane tension as a function of lipid number density in the boundary region ρ_{BR} as shown in Fig. S1. The lipid membrane ruptures and

*To whom correspondence should be addressed

a hole forms at $\rho_{\mathrm{BR}} < 1.0$. As ρ_{BR} increases from 1.0 to 1.45, membrane tension decreases. As Fig. S1 indicates, ρ_{BR} corresponding to a tensionless membrane is around 1.43. At $\rho_{\mathrm{BR}} > 1.5$, the membrane tension becomes negative, and the membrane undergoes strong fluctuation. In the present work, we consider lipid membranes of ρ_{BR} =1.33, 1.43, and 1.53, which correspond to a positive membrane tension, zero membrane tension, and negative membrane tension, respectively.

To analyze the effects of r_{p}/R on the pulling force, we compare f-L curves with $\sigma = 250\kappa/R^2$ at different ratios r_{p}/R in Fig. S2. As r_{p}/R increases, the ratio f/f_0 increases and the f-L curve evolves from a smooth and continuous curve at $r_{\mathrm{p}} = 0$ to a curve exhibiting discontinuous evolution. Similar feature is observed in Fig. 2a at $\sigma = 50\kappa/R^2$ and $150\kappa/R^2$.

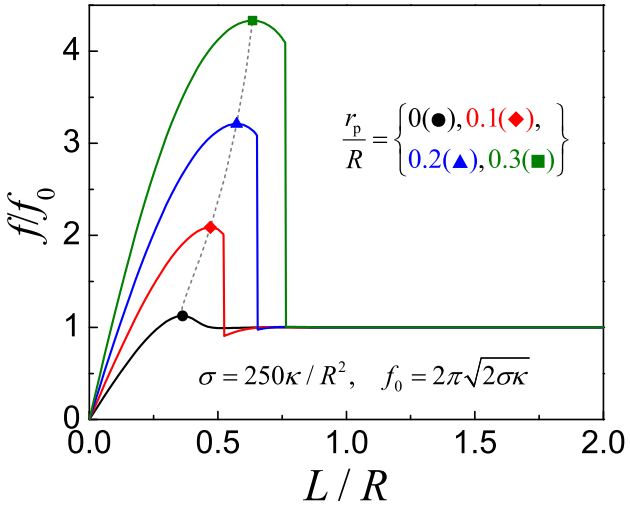

Figure S2: The f-L curves at $\sigma = 250\kappa/R^2$and different nanoplate sizes of r_{p}/R =0, 0.1, 0.2, and 0.3. Solid symbols represent the maximum pulling forces. The (grey) dashed line indicates the relationship between the maximum pulling forces and the corresponding length ratio L/R.

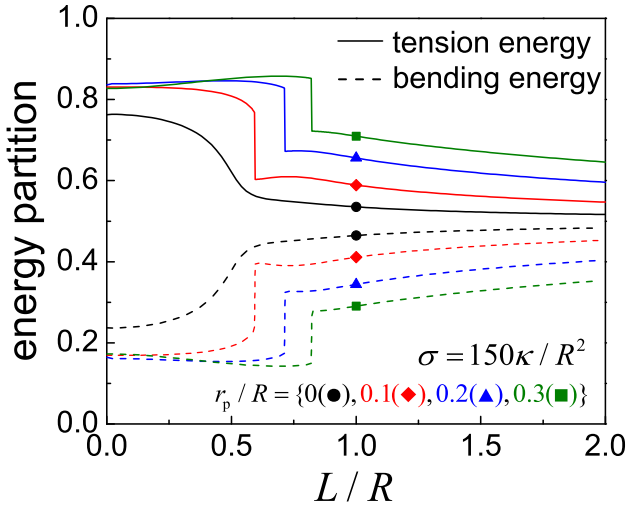

Figure S3: Variations of the membrane tension and bending energy as a function of L/R at $\sigma = 150\kappa/R^2$ and different nanoplate sizes.

Besides the f-L curves, we are also interested in the variation of the membrane tension and bending energy during the pulling process. In Fig. S3, we perform case studies on their variation as a function of L/R at $\sigma = 150\kappa/R^2$. In the early stage of the membrane extraction, tension dominates the membrane deformation and suppresses the large deformation of the membrane. Therefore, no tubule structure but only a cone-shaped configuration is adopted by the extracted membrane. As L/R increases, the bending energy of the membrane plays an increasingly important role as a membrane tubule is formed, though the tension energy still exceeds the bending energy.

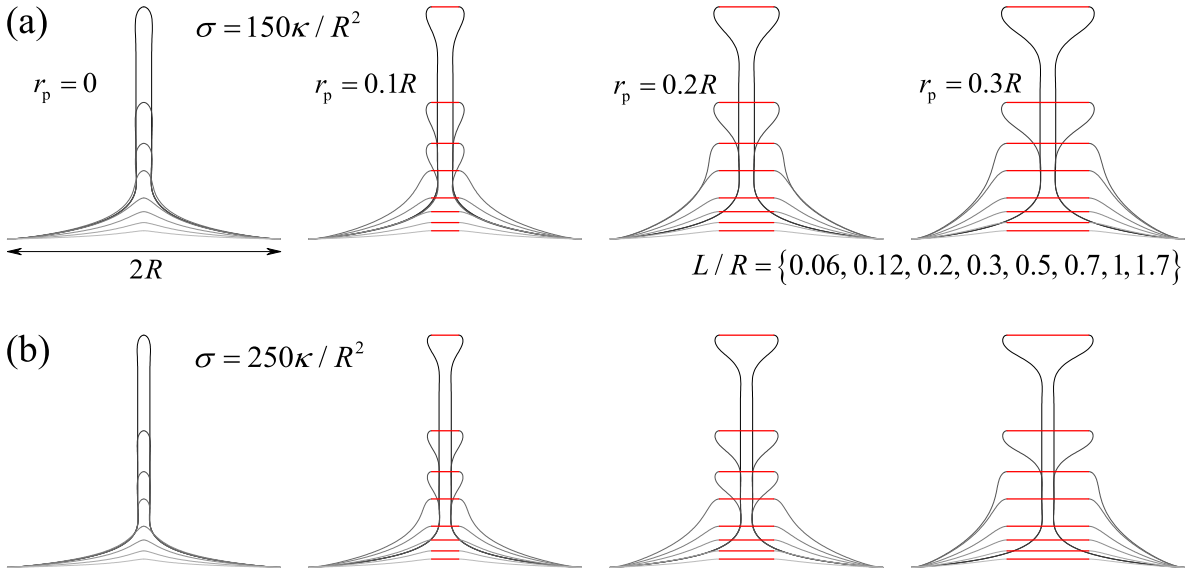

Figure S4: Selected membrane configurations at L/R =0.06, 0.12, 0.2, 0.3, 0.5, 0.7, 1, and 1.7, and different membrane tension $\sigma = 150\kappa/R^2$ (a) and $250\kappa/R^2$ (b) for $r_p/R = 0$, 0.1, 0.2, and 0.3.

The membrane configurations at $\sigma = 50\kappa/R^2$ are provided in Fig. 3 in the main text. Here we plot the configurations at $\sigma = 150\kappa/R^2$ and $250\kappa/R^2$ in Fig. S4a and S4b, respectively. In the case of a point pulling force ($r_p = 0$), the membrane transition as a function of L/R is smooth. As r_0 increases, a discontinuous shape transition is observed. This is consistent with f-L curves in Figs. 2a and S2, where discontinuous force jumps are observed at the finite values of r_p/R. A comparison between Figs. 3 and S4 indicates that a larger membrane tension corresponds to a smaller tether radius independent of r_p, which is expected from the formula $r_0 = \sqrt{\kappa/(2\sigma)}$.

In the main text, the radius of the membrane patch is taken as R. To investigate the effect of the membrane patch size on the tether formation, we perform case studies at the patch radius of $5R$. As shown in Fig. S5, the ratio L/R of the maximum pulling force increases as the membrane size increases but the static pulling force $f_0 = 2\pi\sqrt{2\sigma\kappa}$ is independent of the membrane patch size. As the membrane size increases from R to $5R$, the f-L curve at $r_p = 0.2R$ and $\sigma = 25\kappa/R^2$ evolves from a smooth and continuous curve to a curve exhibiting discontinuous transition.

In Fig. 6 in the main text, we investigate the variation of the lipid number in the transition region and the membrane shape during the pulling process at $v = 0.01$. To explore the effects of pulling velocity on the lipid rearrangement in the transition region and the membrane shape, we calculate the number of lipids in the transition region and the transition angle at different pulling velocities (Fig. 6b and 6c). A larger pulling velocity results in a more rapid nanotube growth (Fig. S6a) and quicker variation of the transition angle (Fig. S6b).

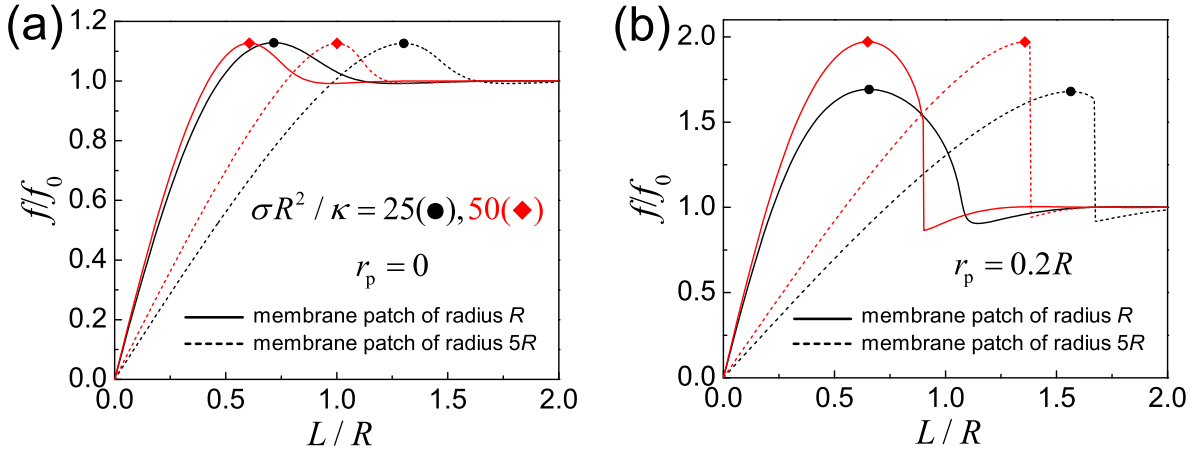

Figure S5: The f-L curves at different membrane sizes and different nanoplate sizes of $r_{\rm p} = 0$ (a) and $0.2R$ (b). The solid symbols represent the maximum pulling forces.

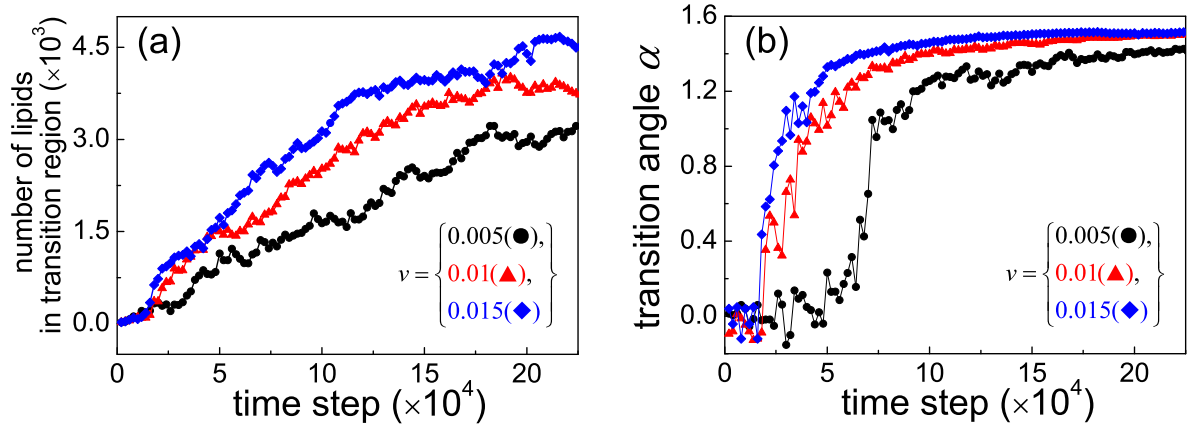

Figure S6: The number of lipids in the transition region and the transition angle α as functions of the time steps at three different pulling velocities $v = 0.005$, 0.01, and 0.015. Here $r_{\rm p} = 8r_{\rm c}$ and $\rho_{\rm BR} = 1.43$.